



Cite this: DOI: 10.1039/c5dt04432d

Received 10th November 2015,
Accepted 25th December 2015

DOI: 10.1039/c5dt04432d

www.rsc.org/dalton

EPR detection and characterisation of a paramagnetic Mo(III) dihydride intermediate involved in electrocatalytic hydrogen evolution†

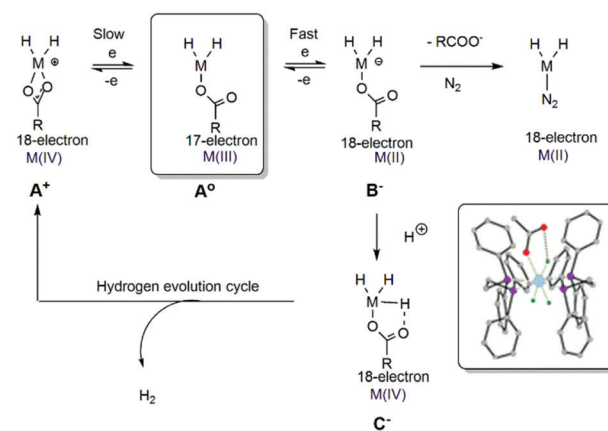
Christopher Prior, Lee R. Webster, Saad K. Ibrahim, Joseph A. Wright, Ali F. Alghamdi, Vasily S. Oganessian* and Christopher J. Pickett*

EPR spectroscopy and theoretical data show that the slow heterogeneous electron-transfer kinetics associated with the reduction of an 18-electron Mo(IV) acetato dihydride are a consequence of an η^2 – η^1 rearrangement of the carboxylate ligand which gives a unique paramagnetic 17-electron Mo(III) dihydride.

The $\{M(\text{Ph}_2\text{PCH}_2\text{CH}_2\text{PPh}_2)_2\}$ platform, where $M = \text{Mo}$ or W and related 1,2-bis(tertiary diphospho)alkane complexes, supports a diverse range of ligand centred chemistry and electrochemistry. This includes protonation of dinitrogen, nitrido, isocyanide and nitrile ligands,^{1–3} oxidation of methyleneamido ligands to cyanide,⁴ reduction of cyanide to the aminocarbyne ligand,⁵ N–N cleavage of dialkylhydrazides,⁶ and electro-synthetic pathways to ammonia, amines and aminoacids.^{7–9} Such platforms also support electrocatalytic hydrogen evolution, for example, the carboxylato-complexes $[\text{MH}_2(\eta^2\text{-RCOO})(\text{Ph}_2\text{PCH}_2\text{CH}_2\text{PPh}_2)_2]^+ \text{A}^+$ ($M = \text{Mo}$; $R = \text{alkyl}$) first reported by Ito and coworkers¹⁰ have been shown to electrocatalyse the reduction of protons to dihydrogen at modest turnover frequencies,^{9,11} and this has been extended to photoelectrocatalysis at semiconductor electrodes.¹² Central to the proposed mechanism for hydrogen evolution, and also to chemistry which leads to the binding of molecular nitrogen or other ligands, is the invocation of a paramagnetic intermediate $[\text{MH}_2(\eta^1\text{-MeCOO})(\text{Ph}_2\text{PCH}_2\text{CH}_2\text{PPh}_2)_2] \text{A}^\circ$ where the η^2 -carboxylate of the parent complex has opened to give an η^1 -ligand, following slow electron-transfer.

Hitherto, only *indirect* experimental evidence has provided support for this rearrangement. Specifically (i) the observation by cyclic voltammetry of a *quasi-reversible* one-electron

reduction whereby the slow heterogeneous kinetics have been taken to signal inner sphere reorganisation concerted with the electron-transfer,¹¹ and (ii) the isolation and X-ray crystallographic characterisation of a stable trihydride $[\text{MH}_3(\eta^1\text{-MeCOO})(\text{Ph}_2\text{PCH}_2\text{CH}_2\text{PPh}_2)_2]$ ($M = \text{W}$) The crystallographic structure of which shows that the carboxylate has an η^1 coordination mode, Scheme 1.^{13,14} This intramolecularly hydrogen-bonded trihydride is formed by ‘trapping’ A° ($M = \text{W}$; $R = \text{Me}$) by a further one electron reduction and protonation, Scheme 1. We now report the detection by EPR (electron paramagnetic resonance) spectroscopy of the key paramagnetic Mo(III) dihydride intermediate A° ($M = \text{Mo}$, $R = \text{Me}$) and its dideuteride analogue, Scheme 1. The fitting of the EPR spectra in combination with rigorous quantum mechanical modelling of the observed spectral features, now provide compelling evidence in support for the ‘open’ carboxylate η^1 -coordination mode in A° , as originally postulated.¹¹ Syntheses and characterisation of the new complexes used in this study together with crystallographic data for A^+ ($M = \text{Mo}$, W ; $R = \text{H}$) are given in the ESI.†



Scheme 1 Summary of electron-transfer chemistry of $[\text{MH}_2(\eta^2\text{-MeCOO})(\text{Ph}_2\text{PCH}_2\text{CH}_2\text{PPh}_2)_2]^+ \text{A}^+$ together with a view of the reported structure of the isolated tungsten trihydride **C** showing the ‘open’ carboxylate form, see ref. 13.

Energy Materials Laboratory, School of Chemistry, University of East Anglia, Norwich Research Park, Norwich NR4 7TJ, UK. E-mail: v.oganesyan@uea.ac.uk, c.pickett@uea.ac.uk

† Electronic supplementary information (ESI) available: Synthesis of $[\text{MH}_2(\text{O}_2\text{CR})(\text{dppe})_2][\text{BPh}_4]$ complexes, spectroscopic characterisation & crystal data, electrochemical and EPR measurements and simulations, DFT computational details. CCDC 1407344 and 1407345. For ESI and crystallographic data in CIF or other electronic format see DOI: 10.1039/c5dt04432d

We first establish the generic *quasi-reversible* behaviour of the $A^{+/0}$ carboxylate couples. The sets of cyclic voltammograms shown in Fig. 1 were recorded at a vitreous carbon electrode in the solvent system $[NBu_4][BF_4]$ -toluene 1 : 3 at 303 K, a solvent of low reactivity in which both redox partners are stable.¹⁵ As is fully consistent with slow heterogenous electron-transfer kinetics, the magnitude of the peak separation ΔE for the $A^{+/0}$ ($M = Mo, R = Me$) couple increases with increasing scan-rate as is illustrated in Fig. 1(a). From this data the standard heterogenous electron-transfer rate constant¹⁶ was determined by

digital simulation¹⁷ to be $k_o^{Mo,Me} = (1.0 \pm 0.1) \times 10^{-4} \text{ cm s}^{-1}$ at 303 K. Corresponding values for the 'fast' reversible ferrocene-ferrocinium couple where solvent reorganisation dominates the heterogenous electron transfer kinetics are typically more than three orders of magnitude faster.¹⁸ The nature of the metal centre influences the electron-transfer kinetics, Fig. 1(b). Thus the electron-transfer rate constant for the tungsten complex under measured under identical conditions, $k_o^{W,Me} = (0.2 \pm 0.02) \times 10^{-4} \text{ cm s}^{-1}$, is about a factor of 5 slower than that for the Mo analogue. This can be attributed to strength of the $M-O_{\text{acetate}}$ bonds which are expected to be greater for W than for Mo. Fig. 1(c) shows a comparison of the voltammograms for complexes $[MH_2(\eta^2-RCOO)(Ph_2PCH_2CH_2PPh_2)_2]^+$ ($M = W; R = Me, H \text{ and } CF_3$). The inductive influence of the carboxylate substituent R clearly has an effect on the magnitude of the formal potential E^0 : the W complex with the more electron-withdrawing $R = CF_3$ group is $510 \pm 10 \text{ mV}$ easier to reduce than is its $R = Me$ analogue. There is also a substantial effect of the substituent group on the electron-transfer kinetics, k_o^{W,CF_3} is about order of magnitude greater than $k_o^{W,Me}$, consistent with a weaker W-O bond and greater lability in the $R = CF_3$ complex. Heterogenous electron-transfer rate constants for these systems together with parameters used in the simulations are tabulated in the ESI.†

The reduction of the dihydride A^+ ($M = Mo; R = Me$) was carried out in the cavity of an EPR spectrometer by controlled-potential electrolysis at a platinum wire working electrode in tetrahydrofuran containing 0.2 M $[NBu_4][BF_4]$ as the supporting electrolyte under an atmosphere of argon. The potential was set at the onset of reduction of the complex. The room temperature EPR spectra obtained by reduction of both A^+ ($M = Mo, R = Me$) and its 2H analogue are shown as black lines in Fig. 2(a) and (b), respectively. There is a considerable difference between their EPR lineshapes. Both spectra were fitted using the fast motional regime model as implemented in Easy-spin software¹⁹ and the adjusted parameters are summarized in Table 1.

Analysis reveals that the EPR spectra result from large hyperfine coupling to four phosphorous nuclei in a 1 : 4 : 6 : 4 : 1 pattern, with further splitting from the hydrides in a 1 : 2 : 1 pattern. Since the isotropic coupling constants of phosphorous is about twice that of the hydrides, in A^0 the internal lines from the hydride splitting overlay giving eleven discernible lines instead of fifteen. Upon deuteration, the hydrogen splitting is reduced by the magnetogyric ratio, γ_D/γ_H , ($A_{\text{Iso}}(^1H) = -39.1 \text{ MHz}/A_{\text{Iso}}(^2H) = -7.3 \text{ MHz}$) to a magnitude where it is not resolved due to line broadening, leaving only the splitting pattern from the phosphorous nuclei. The acetate group has negligible interactions with the spin system. In the simulations the negative signs of the major A_{Iso} ($^{31}P, H$) components were assigned on the basis of a slight increase in line-width across the spectra, with the low magnetic field $m_I = -I$ line being marginally narrower than that of the high magnetic field $m_I = +I$ feature. This was confirmed by an increase in the accuracy of fitting when using negative values as well as the DFT calculations.

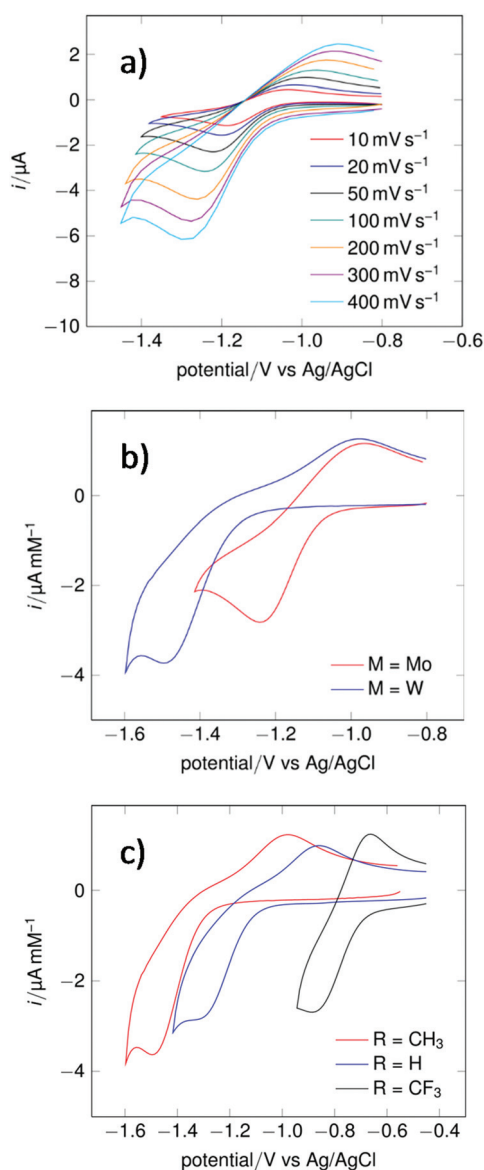


Fig. 1 Cyclic voltammograms for the $[MH_2(\eta^2-RCOO)(Ph_2PCH_2CH_2PPh_2)]^+$ complexes recorded at 303 K at a vitreous carbon electrode, area 0.071 cm^2 , in $[NBu_4][BF_4]$ -toluene 1 : 3 molar ratio. (a) Scan rate dependence for $M = Mo; R = Me$ (b) complexes $M = Mo$ and $W; R = Me$ at 100 mV s^{-1} (c) complexes $M = W; R = Me, H \text{ and } CF_3$ at 100 mV s^{-1} .

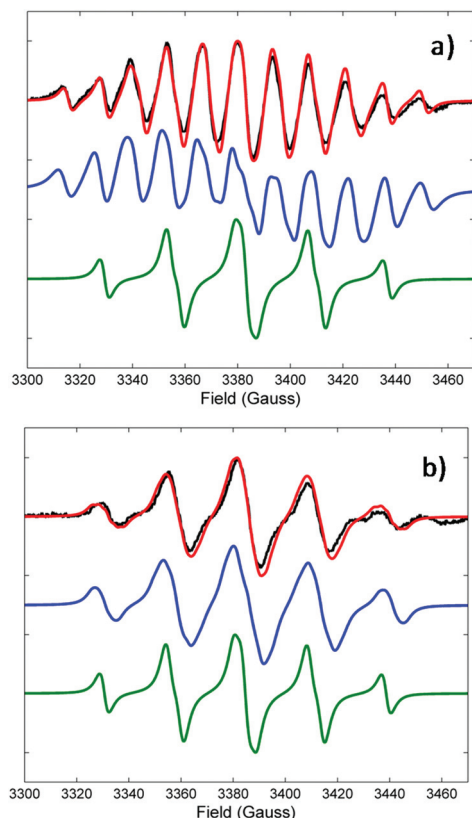


Fig. 2 EPR spectra of A° (a) and its deuterated form (b). In each panel black, red and blue lines correspond to experimental, fitted and predicted from DFT spectra, respectively. Spectra obtained with hydrogen and deuterium hyperfine couplings excluded from the EPR simulation are shown by green lines.

Table 1 Comparison between magnetic parameters obtained from the fitting of EPR spectra with those predicted from DFT.²³ Isotropic hyperfine coupling constants are given in MHz

Parameter	EPR	DFT C_1
g_{iso}	2.016	2.039
$A_{\text{iso}} (^{31}\text{P})$	−82.2 −78.9 −73.0 −69.2	−88.83 −78.05 −76.05 −66.19
$A_{\text{iso}} (^1\text{H})$	−37.8 −40.4	−38.4 −38.5
$A_{\text{iso}} (^2\text{H})$	−7.4 −7.3	−6.0 −6.0

EPR measurements indicate that the unpaired electron is essentially located on the metal centre. The effect is particularly noticeable in the extended EPR spectrum of the deuterated form of A° where hyperfine splitting from hydrides is reduced. The contributions from Mo to the hyperfine occur from the Mo^{95} ($I = 5/2$, 15.92%) and Mo^{97} ($I = 5/2$, 9.55%) isotopes and result in characteristic low intensity features visible either side of the five lines arising from phosphorous splitting

(see Fig. S2 of ESI†). The fitted value of 78 MHz for the hyperfine coupling contribution from Mo is in excellent agreement with previous reports on organodiazenido Mo complexes.²⁰

The structure of complex A° was optimized using DFT calculations (Gaussian 09²¹) followed by prediction of magnetic parameters (A and g) (details are provided in ESI†). The complex was found to be of C_1 symmetry, with two phosphorous atoms distorted slightly out of the molecular plane, with opposite positions distorted in the same direction in a two up two down arrangement (Fig. 3). The hydrides were slightly rotated away from the linear P–Mo–P axis. Importantly, upon reduction of the complex from 18-electron system (diamagnetic state) to the 17-electron system (paramagnetic state) the orientation of the COOCH_3 ligand with respect to Mo changes from fully symmetric (Scheme 1) to one in which a single O atom is bound to Mo with an Mo–O–C angle of $\sim 125^\circ$. The core structure of A° is presented in Fig. 3 with full atomic coordinates provided in ESI.† Magnetic parameters calculated from DFT are summarized in Table 1 and are compared with the ones obtained from the fitting of EPR spectra. There is a perfect agreement for the A values of both ^1H and ^2H . The distribution of the isotropic phosphorous coupling constants is consistent between the fitted values and DFT, including the signs. As often reported for paramagnetic complexes containing phosphorous atoms, the predicted isotropic ^{31}P couplings are underestimated compared to experimental ones.²² Thus a factor of ~ 1.44 , which is in agreement with previous DFT studies of Mo–P complexes,²² has been used to scale the P

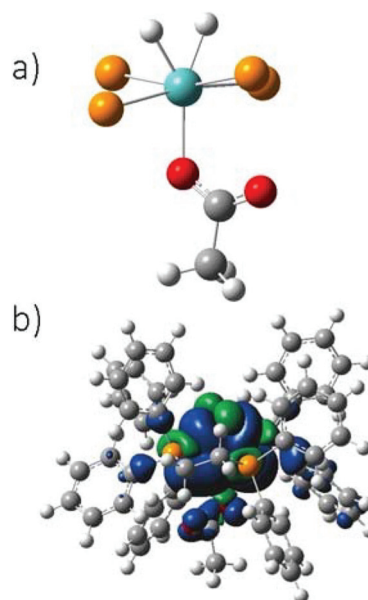


Fig. 3 DFT optimized structures of $[\text{MoH}_2(\eta^1\text{-CH}_3\text{COO})(\text{Ph}_2\text{CH}_2\text{CH}_2\text{Ph}_2)_2]^0$ (a) core $\{\text{MoP}_4\text{H}_2\text{OC}=\text{OCH}_3\}$ arrangement showing deployment of acetate group in η^1 -configuration [orange = P; blue = Mo; white = H; grey = C] (b) isosurfaces of the spin density distribution of complex A° . Green and blue show the two phases of the spin-density distribution. Note spin density for the hydrides in the apical positions (green).

hyperfine coupling values. The EPR spectra predicted using the parameters calculated by DFT are shown in Fig. 2 as middle (blue) lines in panels (a) and (b) for \mathbf{A}° and its ^2H analogue, respectively, demonstrating a good agreement with hydrides. The impact of the hydrogen and deuterium hyperfine couplings on the EPR lineshapes can be clearly seen by excluding their relevant contributions from the EPR simulation. The results are presented as green curves in Fig. 2(a) and (b) for \mathbf{A}° and its ^2H analogue, respectively.

DFT calculations indicate that spin density in all systems is primarily localized on the molybdenum centre (Fig. 3), which accounts for 62% of the total unpaired spin density. The P atoms bear a considerable spin density (a total of 12%) and $\sim 1\%$ of the density resides on the nearest to Mo O atom. The hydrides are characterized by large s-orbital spin density ($\sim 3.0\%$ per hydride) due to the direct interaction with molybdenum, being roughly equal to the total s orbital spin density of all the phosphorous atoms (calculated with standard isotropic atomic hyperfine coupling values).²⁴

Both experimental EPR spectra and DFT calculations lead to a conclusion that two H atoms in complex \mathbf{A}° are ligated to Mo ion and possess strong hyperfine coupling. The Mo–H distance is 1.74 Å and the H–Mo–H angle is $\sim 60^\circ$ (see Table 2). The results for complex \mathbf{A}° are also consistent with our recent study on a paramagnetic μ -hydride di-iron dithiolate complex with significant hyperfine coupling on the single bridging hydride ($A_{\text{iso}} \sim -75$ MHz).²⁵ The values of both $A_{\text{iso}}(\text{P})$ and $A_{\text{iso}}(\text{H})$ hyperfine couplings are also consistent with the relevant values reported for a paramagnetic Mo(v) polyhydride complex.²⁶

Spectroscopic and theoretical data show that the slow heterogeneous electron-transfer kinetics associated with the single electron reduction of the Mo(IV) 18-electron dihydride are now fully explained by a concerted $\eta^2\text{-}\eta^1$ rearrangement of the carboxylate co-ligand. This gives the 17-electron Mo(III) dihydride intermediate avoiding the formation of a high energy 19-electron species. Paramagnetic molybdenum and tungsten hydrides are rather rare and largely confined to more or less unstable Mo(v) species.²⁷ Only one example of a Mo(III) hydride species has been spectroscopically characterized, an

unstable monohydride reported by Schrock and co-workers,²⁸ the Mo(III) dihydride detected herein is unique.

We thank Taibah University, Saudi Arabia, for funding Dr Ali Alghamdi to undertake a period of research at the Energy Materials Laboratory. The EPSRC is thanked for providing postgraduate studentship to LRW. The EPSRC is thanked for supporting this work through grants to CJP (EP/H019480/1) and VSO (EP/L001322/1). We gratefully acknowledge the EPSRC UK National Crystallography Service at the University of Southampton for the collection of the crystallographic data.²⁸

Notes and references

- 1 J. Chatt, J. R. Dilworth and R. L. Richards, *Chem. Rev.*, 1978, **78**, 589–625.
- 2 R. A. Henderson, G. J. Leigh and C. J. Pickett, *Adv. Inorg. Chem. Radiochem.*, 1983, **27**, 197–292.
- 3 H. Seino, Y. Mizobe and M. Hidai, *Chem. Rec.*, 2001, **1**, 349–361.
- 4 A. Hills, D. L. Hughes, C. J. Macdonald, M. Y. Mohammed and C. J. Pickett, *J. Chem. Soc., Dalton Trans.*, 1991, 121–129.
- 5 D. L. Hughes, S. K. Ibrahim, H. M. d. Ali and C. J. Pickett, *J. Chem. Soc., Chem. Commun.*, 1994, 425–427.
- 6 R. A. Henderson, G. J. Leigh and C. J. Pickett, *J. Chem. Soc., Dalton Trans.*, 1989, 425–430.
- 7 C. J. Pickett, *J. Biol. Inorg. Chem.*, 1996, **1**, 601–606.
- 8 C. J. Pickett and J. Talarmin, *Nature*, 1985, **317**, 652–653.
- 9 D. L. Hughes, S. K. Ibrahim, C. J. Macdonald, H. M. Ali and C. J. Pickett, *J. Chem. Soc., Chem. Commun.*, 1992, 1762–1763.
- 10 T. Ito, A. Takahashi and S. Tamura, *Bull. Chem. Soc. Jpn.*, 1986, **59**, 3489–3494.
- 11 D. L. Hughes, S. K. Ibrahim, C. J. Pickett, G. Querne, A. Laouenan, J. Talarmin, A. Queiros and A. Fonseca, *Polyhedron*, 1994, **13**, 3341–3348.
- 12 L. R. Webster, S. K. Ibrahim, J. A. Wright and C. J. Pickett, *Chem. – Eur. J.*, 2012, **18**, 11798–11803.
- 13 S. A. Fairhurst, R. A. Henderson, D. L. Hughes, S. K. Ibrahim and C. J. Pickett, *J. Chem. Soc., Chem. Commun.*, 1995, 1569–1570.
- 14 R. A. Henderson, S. K. Ibrahim, K. E. Oglieve and C. J. Pickett, *J. Chem. Soc., Chem. Commun.*, 1995, 1571–1572, DOI: 10.1039/C39950001571.
- 15 C. J. Pickett, *J. Chem. Soc., Chem. Commun.*, 1985, 323–326.
- 16 A. D. Clegg, N. V. Rees, O. V. Klymenko, B. A. Coles and R. G. Compton, *J. Electroanal. Chem.*, 2005, **580**, 78–86.
- 17 M. Rudolph, *DigiElch 4.0*, Germany, Elchsoft, 2006.
- 18 L. Xiao, E. J. F. Dickinson, G. G. Wildgoose and R. G. Compton, *Electroanalysis*, 2010, **22**, 269–276.
- 19 S. Stoll and A. Schweiger, *J. Magn. Reson.*, 2006, **178**, 42–55.
- 20 G. Butler, J. Chatt, G. J. Leigh and C. J. Pickett, *J. Chem. Soc., Dalton Trans.*, 1979, 113–116.
- 21 M. J. Frisch, *et al.*, *GAUSSIAN 09 (Revision C01)*, Gaussian Inc., Wallingford CT, 2009.

Table 2 Selected structural parameters (distances and angles) of the DFT optimised complex \mathbf{A}°

Parameter	DFT
Mo–P	2.47 Å 2.49 Å 2.50 Å 2.49 Å
H–H	1.71 Å
Mo–H	1.74 Å 1.73 Å
H–Mo–H	59.0°
Mo–O	2.19 Å
Mo–O–C	125.0°

- 22 H. Sidorenkova, T. Berclaz, B. Ndiaye, A. Jouaiti and M. Geoffroy, *J. Phys. Chem. Solids*, 2009, **70**, 713–718.
- 23 Since in the fast motional regime the averaged g value has only a systematic shift effect on the EPR spectrum in all simulated spectra its fitted value was employed. (b) A scaling factor of 1.44 was applied for the Aiso (^{31}P) values predicted from DFT (see text).
- 24 J. E. Wertz and J. R. Bolton, *Electron spin resonance: elementary theory and practical applications*, McGraw-Hill, New York, 1972.
- 25 A. Jablonskyte, J. A. Wright, S. A. Fairhurst, J. N. T. Peck, S. K. Ibrahim, V. S. Oganessian and C. J. Pickett, *J. Am. Chem. Soc.*, 2011, **133**, 18606–18609.
- 26 D. L. Hughes, D. J. Lowe, M. Y. Mohammed, C. J. Pickett and N. M. Pinhal, *J. Chem. Soc., Dalton Trans.*, 1990, 2021–2027.
- 27 B. Pleune, D. Morales, R. Meunier-Prest, P. Richard, E. Collange, J. C. Fettingier and R. Poli, *J. Am. Chem. Soc.*, 1999, **121**, 2209–2225.
- 28 R. A. Kinney, D. G. H. Hetterscheid, B. S. Hanna, R. R. Schrock and B. M. Hoffman, *Inorg. Chem.*, 2010, **49**, 704–713.